ISSN 0031-918X, The Physics of Metals and Metallography, 2016, Vol. 117, No. 4, pp. 390–398. © Pleiades Publishing, Ltd., 2016.
Original Russian Text © M.V. Odnobokova, A.Yu. Kipelova, A.N. Belyakov, R.O. Kaibyshev, 2016, published in Fizika Metallov i Metallovedenie, 2016, Vol. 117, No. 4, pp. 404–413.

STRENGTH AND PLASTICITY

Mechanical Behavior and Brittle–Ductile Transition of High-Chromium Martensitic Steel

M. V. Odnobokova, A. Yu. Kipelova, A. N. Belyakov, and R. O. Kaibyshev

Belgorod National Research University, ul. Pobedy 85, Belgorod, 308015 Russia

e-mail: odnobokova@bsu.edu.ru

Received July 21, 2015; in final form, October 23, 2015

Abstract—The article presents data on the static tensile tests and dynamic impact-toughness tests of a high-chromium martensitic 10Kh9V1M1FBR steel (0.12 wt % C, 9.8 wt % Cr, 0.93 wt % W, 1.01 wt % Mo, 0.2 wt % V, 0.05 wt % Nb, 0.05 wt % N, 0.003 wt % B, 0.36 wt % Mn, 0.2 wt % Ni, 0.06 wt % Si, 0.01 wt % P, 0.008 wt % S, 0.02 wt % Cu, 0.1 wt % Co, 0.015 wt % Al, and the remainder is Fe) in the temperature range from 20 to −196°C. In the case of static loading, a reduction in the temperature leads to an increase in the strength characteristics; upon a drop in the temperature from 20 to −100°C, the plasticity also increases. This is connected with the fact that the ductile fracture remains the basic mechanism down to cryogenic temperatures. The brittle–ductile transition related to the transition from ductile intragranular fracture to quasi-brittle one is observed at −45°C. The steel exhibits high impact toughness to the temperature of −60°C (KCV_{-60} = 95 J/cm^2), at which the fraction of the ductile component in fracture is equal to 20%. At 80°C, the impact toughness decreases down to critical values (30 J/cm^2), which correlates with the decrease in the fraction of the ductile component on the fracture surface down to 1%. The further decrease in the impact toughness down to 10 J/cm^2 at −196°C is related to the transition from intragranular to intergranular brittle fracture.

Keywords: martensitic steel, impact toughness, microstructure, brittle–ductile fracture, fractography

DOI: 10.1134/S0031918X16040098

INTRODUCTION

Martensitic steels with 9–12% Cr are widely used for producing elements for coal-fired power plants operating at steam temperature up to 630°C due to their unique heat resistance [1, 2]. Moreover, they are not susceptible to strong embrittlement during long-term operation, unlike austenitic steels [1, 3–6]. This ensures the reliable operation of high-temperature circuits of boilers and main steam pipes, and allows one to evaluate the residual life of these units with high accuracy [1, 6]. In addition, the low temperature of the brittle–ductile transition (BDT) and the high impact toughness ensure the high reliability of the operation of steam-turbine rotors [1].

In the last 15 years, high-chromium steels are widely used and are considered to be promising material for various parts of thermal reactors and fast-neutron reactors that belong to the third and fourth generations, respectively [7–10]. Neutron irradiation leads to an increase in the temperature of the BDT up to 200–300°C and to a decrease in the high-temperature impact toughness [8, 9]. The low temperature of the BDT and the high values of the impact toughness are critical requirements for the 9–12% Cr steels used in atomic power industry, especially, for steels strengthened by nanoparticles of oxides [8–11].

Despite the importance of the above parameters (the impact toughness and the temperature of the BDT) for the practical application of high-chromium steels [1], a detailed study was only performed in a limited number of works [3–6, 12–17] and none of them were devoted to the mechanisms responsible for the BDT. Thus, our work is aimed at a detailed analysis of the BDT and of the mechanical behavior of one of the most common modern high-chromium steel 10Kh9V1M1FBR (Russian analog of the European E911 steel) at cryogenic temperatures [1]. This steel is used as material for pipes of boilers and the main steam pipe, as well as for the rotors of steam turbines. Impact tests for a detailed analysis of the BDT of this material were carried out simultaneously with static tensile tests in the temperature range from −196 to 20°C. These complex studies allow one to estimate the effect of the loading rate on the fracture toughness.

Brittle–Ductile Transition at Static and Impact Loadings

The rate of loading steels affects the BDT in accordance with the well-known scheme (Fig. 1) [18]. In general, the shift of the BDT temperature increases with increasing loading rate. The difference between

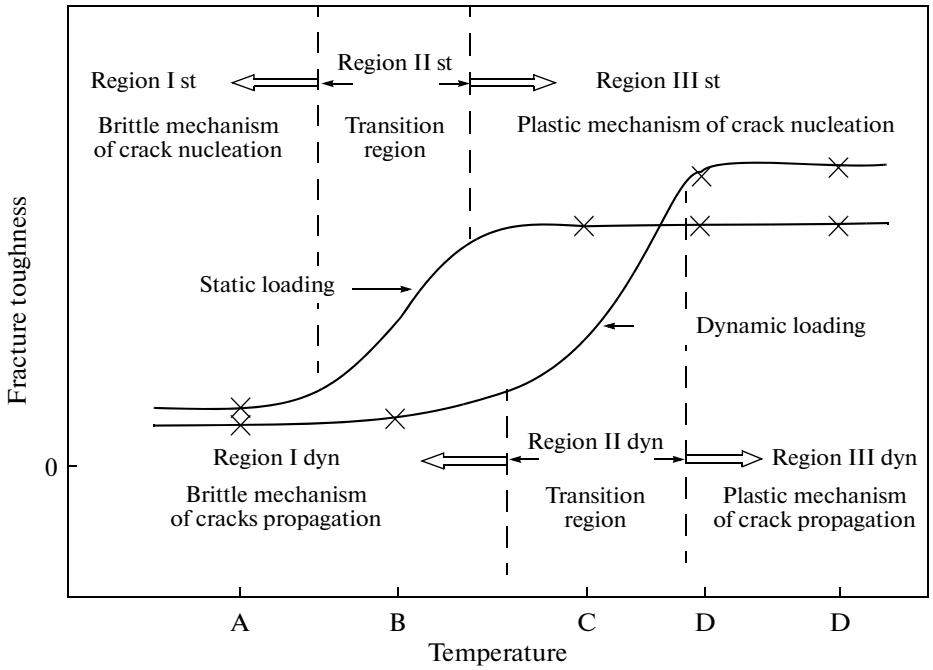

Fig. 1. Dependence of the fracture toughness on the temperature upon static and dynamic loading [18].

the temperatures of the BDT obtained in impact tests and in static tensile tests depends on the yield strength and, for most steels, is described by the equation [18]

$$\Delta T_{\mathrm{BDT}} = 100 - 1.2\sigma_{0.2}, \quad (1)$$

where ΔT_{BDT} is the difference between the temperatures of the BDT at static tensile tests and impact tests (°C), while $\sigma_{0.2}$ is the yield stress at room temperature (MPa). This relation is performed well for most steels with a yield stress of 193–931 MPa. In steels with $\sigma_{0.2} \geq 931$ MPa, the difference in the temperatures of the BDT between the static tensile and impact toughnesses is absent [18]. The dependence of the fracture toughness on the temperature at the static and impact loading relates to the mechanisms of nucleation and propagation of cracks (Fig. 1) [18].

The using of Charpy standard specimens with a V-shaped notch provides for the value of intensity stress at the crack tip to be above the critical value K_c of the material and leads to the unstable propagation of the crack after fairly short stages of nucleation and stable growth of the crack with a size less than the critical one [18]. At the static and impact loadings, in regions I (temperature A) and III (temperature D), the nucleation and propagation of crack occurs via the mechanisms of brittle and plastic fracture, respectively [18]. In transition region II, upon static loading (temperature B) and impact loading (temperature C), the crack nucleates via a plastic mechanism and propagates by brittle fracture.

EXPERIMENTAL

The investigations were carried out using 10Kh9V1M1FBR steel with the following chemical composition: 0.12 wt % C, 9.8 wt % Cr, 0.93 wt % W, 1.01 wt % Mo, 0.2 wt % V, 0.05 wt % Nb, 0.05 wt % N, 0.003 wt % B, 0.36 wt % Mn, 0.2 wt % Ni, 0.06 wt % Si, 0.01 wt % P, 0.008 wt % S, 0.02 wt % Cu, 0.1 wt % Co, 0.015 wt % Al, and the remainder was Fe. The samples were subjected to normalization from 1060°C with subsequent two-stage tempering at 300 and 760°C for 3 h at each temperature. The fine structure and the chemical and phase compositions of the second phases after tempering were studied using a JEOL-2100 transmission electron microscope (TEM) at an accelerating voltage of 200 kV, which was equipped with an attachment for energy dispersive microanalysis (Oxford Instruments).

TEM foils were prepared by a jet electropolishing method using a 10% solution perchloric acid in acetic acid in a Struers Tenupol-5 device. To obtain the precise chemical composition of the particles of second phases, carbon replicas obtained by sputtering carbon onto the prepolished and etched surface of samples with the subsequent etching of the metal matrix using a 10% solution of hydrochloric acid in ethanol at a voltage of 2V were studied.

The transverse size of the martensite laths was calculated by the intercept method using TEM images. The dislocation density was determined by counting the individual dislocations inside the martensite laths using typical TEM images. The average size of second-phase particles was measured using TEM images.

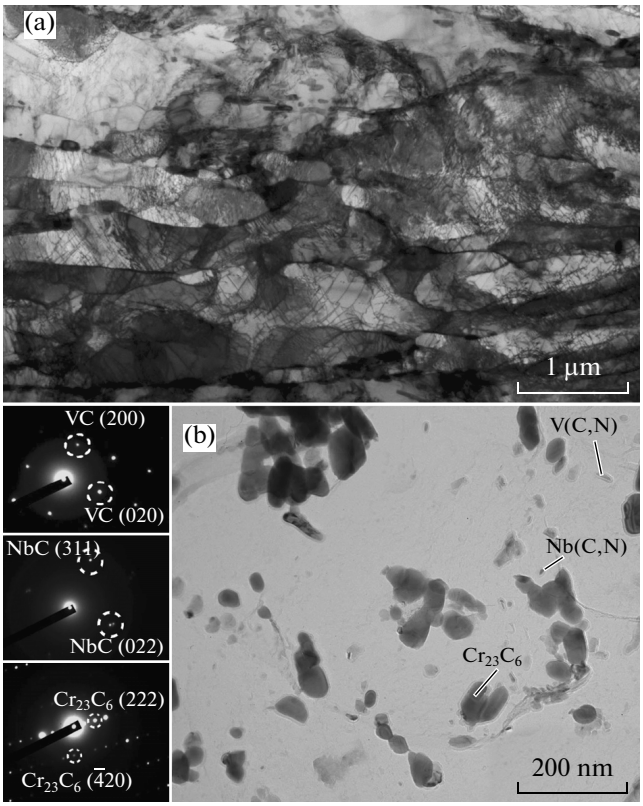

Fig. 2. (a) Microstructure, (b) particles of carbides and carbonitrides on the carbon replicas of 10Kh9V1M1FBR steel after normalization from 1060°C and two-stage tempering at 300 and 760°C.

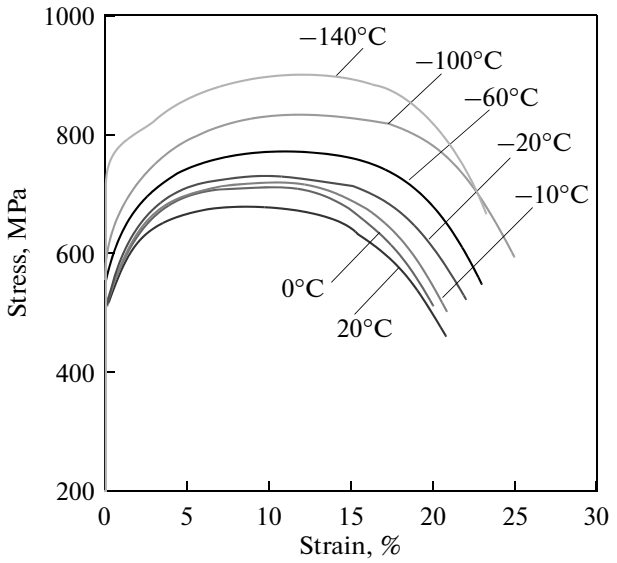

Fig. 3. Engineering stress–strain curves of 10Kh9V1M1FBR steel upon mechanical tensile tests in the temperature range from 20 to −140°C.

The tensile tests were performed using flat samples with a length of the working part of 35 mm and a cross section of 3 × 7 mm in an Instron 5882 universal testing machine at temperatures of 20, 0, −10, −20, −60, −100, and −140°C at a deformation rate of 2 mm/min. The impact tests were carried out using standard samples with a square section of 10 × 10 mm, length of 55 mm, and a V-shaped stress concentrator using an Instron IMP 460 pendulum impact machine at temperatures of 20, 0, −20, −40, −60, −80, and −196°C.

After mechanical tests, the fractometric studies were carried out using an FEI Quanta 600F scanning electron microscope. The fraction of the plastic component in the fracture of the samples after impact tests at different temperatures and at the temperature of the BDT, i.e., the fracture appearance transition temperature (FATT), was determined by the fraction of the plastic component, which was calculated according to ASTM E 23-07a.

RESULTS

Microstructure of Steel after Two-Stage Tempering

10Kh9V1M1FBR steel after normalization and two-stage tempering has a structure typical of high-chromium martensitic steels (troostomartensite structure) with an average transverse size of the laths of packet martensite of 0.335 μm (Fig. 2a). A high dislocation density (~5×10^{14} m^{-2}) is observed within the martensite laths. During tempering, the precipitation of $M_{23}C_6$-type carbides with an average size of 100–150 nm occurs at the boundaries of the initial austenite grains (IAGs), martensite packets, and blocks (Fig. 2a).

M(C,N) carbonitrides enriched in niobium and vanadium, which are clearly differ in their morphology, are distributed uniformly over the entire volume of the steel [12]. The niobium-enriched carbonitride particles have a round shape with an average size of about 5–10 nm. The vanadium-enriched carbonitride particles have a platelike shape with an average length of 50 nm and width of 10 nm (Fig. 2b). Therefore, 10Kh9V1M1FBR steel demonstrates a two-phase separation of the *M*(C,N) carbonitrides into niobium- and vanadium-enriched carbonitrides, which provides their stability against coalescence at high temperatures [1, 12, 19, 20].

Mechanical Properties

Figure 3 shows the engineering stress–strain curves (tensile diagrams). The values of the ultimate tensile strength (σ_u), yield stress ($\sigma_{0.2}$), relative elongation (δ), and uniform elongation (δ_u) obtained as the result of tests are presented in the table.

The shape of $\sigma-\varepsilon$ curves at all test temperatures is approximately the same. At the initial stage of deformation, noticeable strain hardening is observed, which gradually goes into a long stage of stable flow.

Effect of the test temperature on the yield stress ($\sigma_{0.2}$), ultimate tensile strength (σ_u), relative elongation (δ), and uniform elongation (δ_u)

Mechanical properties	Test temperature, °C						
	20	0	−10	−20	−60	−100	−140
σ_u, MPa	675	710	715	730	770	830	900
$\sigma_{0.2}$, MPa	500	500	510	520	545	590	710
δ, %	21	20	21	22	23	25	23
δ_u, %	9.5	10	10.5	11	12	14	13

The localization of deformation, which leads to the formation of a neck (Fig. 4), occurs at the stage of apparent softening. Thus, the fracture of samples occurs after significant uniform elongation at all test temperatures (table).

The $\sigma_u/\sigma_{0.2}$ ratio varies from 1.35 to 1.42, which provides high stability of the plastic flow and high uniform elongation. A reduction in temperature leads to an increase in both the strength characteristics and plasticity. The plasticity only begins to decrease at $T <$ −100°C. With a decrease in the test temperature from 20 to −140°C, the yield stress increases from 500 to 710 MPa. The relative elongation is in the range of 20–15%. Thus, the steel shows no signs of BDT upon a reduction in the test temperature to cryogenic temperatures.

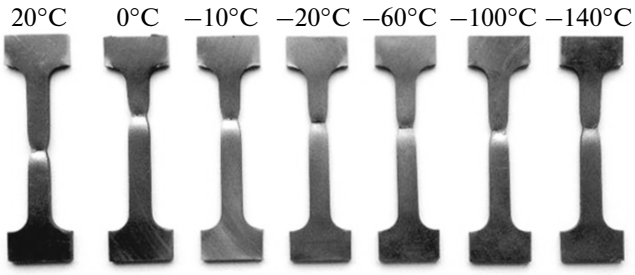

Fig. 4. Samples of 10Kh9V1M1FBR steel after mechanical tensile tests in the range of temperatures from 20 to −140°C.

Impact Toughness

The results of impact tests of 10Kh9V1M1FBR steel are presented in Fig. 5. The steel exhibits a clearly pronounced BDT at −45°C. With a reduction in the test temperature from 0 to −80°C, an almost linear drop in the values of the impact toughness from 230 to 30 J/cm^2 is observed (Fig. 5a). Note that the steel exhibits a high impact toughness at temperatures down to −60°C, at which its *KCV* is 95 J/cm^2. The value of the impact toughness decreases by a factor of three with decreasing temperature from −60 to −80°C. However, even at this temperature, *KCV* = 30 J/cm^2. This value is considered sufficient to stop the fracture at a crack propagation upon dynamic loading and exceeds 20 J/cm^2, which is a conditional boundary of the transition from plastic to brittle fracture [18]. At a subsequent decrease in the test temperature down to −196°C, there is a further reduction in

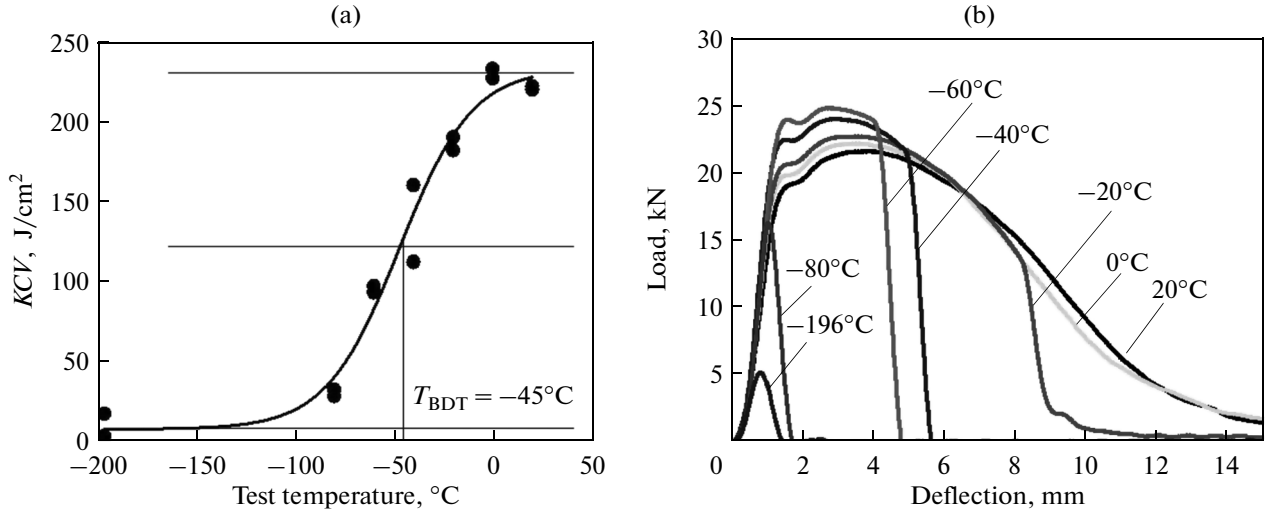

Fig. 5. (a) Dependence of impact toughness on test temperature and (b) load–deflection curves at different temperatures.

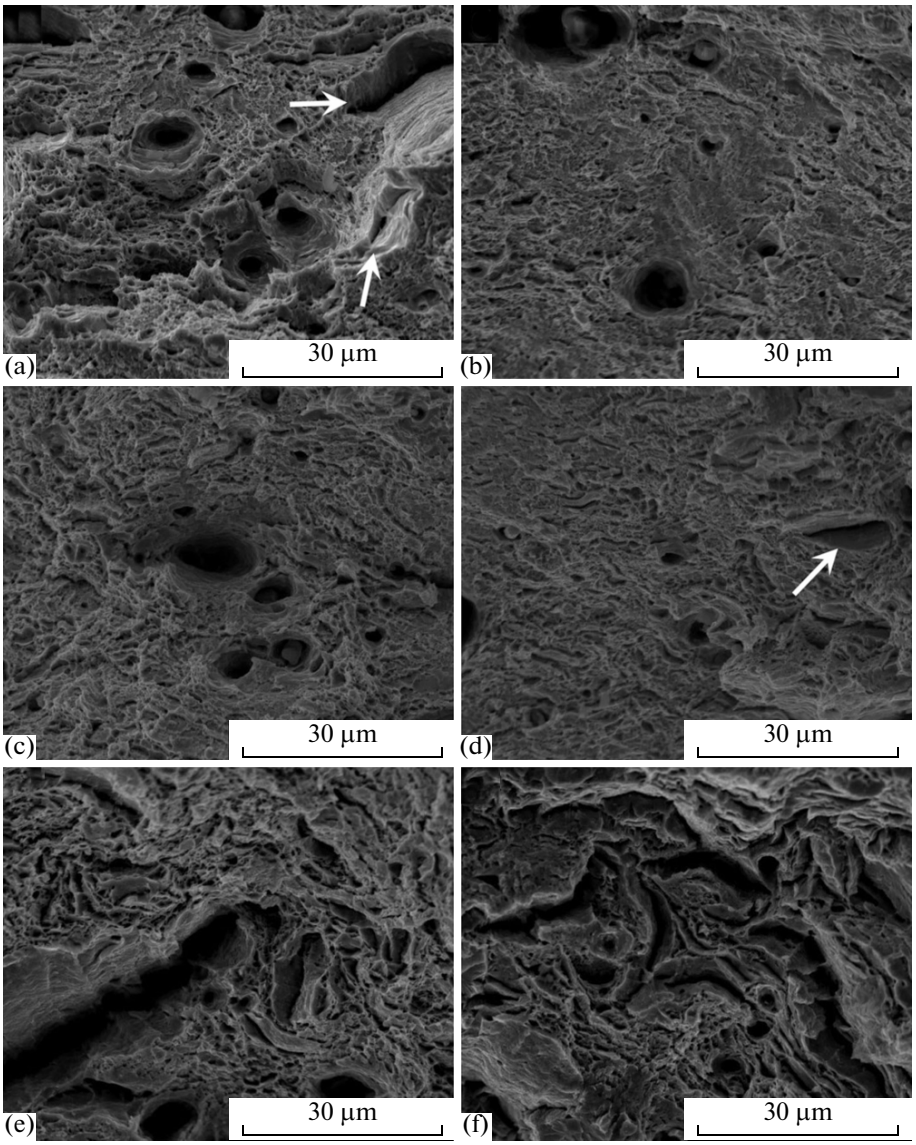

Fig. 6. Fractography of fractures of 10Kh9V1M1FBR steel after tensile tests at temperatures of (a) 20 , (b) 0, (c) −20, (d) −60, (e) −100, and (f) −140°C.

the impact toughness down to 10 J/cm^2. Thus, the steel is only completely embrittled at the temperature of liquid nitrogen.

The analysis of the fracture curves (Fig. 5b) shows that the reduction in the test temperature in the range of 20 to −60°C increases the load and fracture occurs in the region of plastic deformation. This increase in the load is correlated with an increase in the stress upon static loading and shows that the fracture in this temperature range occurs after large plastic deformation. At a temperature of −20°C and above, the region of plastic deformation exceeds the sample thickness, which allows us to talk about the so-called hinge fracture when the path of crack propagation prior to the separation of the sample into two parts is much longer than the thickness of the Charpy sample [18, 21]. The crack only propagates through the thickness of the sample at temperature of −40°C and below. The transition to brittle fracture without the formation of a plastic zone occurs at −80°C. At this temperature and below, the propagation of the crack begins to outpace the pendulum motion, i.e., the crack propagation occurs due to the relaxation of the elastic energy [18]. At −196°C, the mechanism of brittle fracture becomes different, since the load required to start the propagation of a main crack decreases by more than three times.

Fractography

Figure 6 presents fractographs of fractures in 10Kh9V1M1FBR steel after tensile test. An analysis of the fracture surface in the central part of the samples

(zone of nucleation and slow propagation of the crack) shows a single-type plastic fracture in the temperature range of 20 to −60°C (Figs. 6a–6d). In this temperature range, plastic intragranular fracture via the nucleation, growth, and coalescence of micropores prevails. The majority of fracture surfaces is represented by fine, deep dimples with diameters of less than 5 μm and a few coarse dimples with sizes of 10–20 μm, most of which have particles at the bottom. The nucleation of the coarse dimples mostly occurs at the interfaces between the matrix and dispersed particles. The majority of these coarse pores [22] are located at the boundaries of the IAGs. The coalescence of these pores leads to the formation of "canyons" at the grain boundaries (indicated by arrows in Figs. 6a and 6d). Consequently, in this case, intergranular plastic fracture occurs. However, this mechanism is not important, since the pores formed at grain-boundary particles grow in isolation and only form elongated cracks in some cases, the size of which is significantly less than critical.

The fraction of the canyons increases with a decrease in the test temperature to −100 and −140°C. The canyons nucleate at the boundaries of the IAGs and martensite packets (Figs. 6e and 6f). The round pores of large size are formed by the mechanism of plastic fracture; the elongated pores, by the mechanism of quasi-cleavage [22]. The presence of slip lines on their walls indicates that severe plastic deformation occurs upon the formation of surfaces. In general, with decreasing test temperature, the fraction of intergranular fracture increases and the transition from plastic fracture to quasi-cleavage occurs. However, even at −140°C, plastic intragranular fracture is the predominant mechanism. Correspondingly, the fracture surface of the samples tested at these temperatures represents the alternation of canyons and coarse dimples formed at the boundaries of IAGs and martensite packets, as well as shallow dimples in the bulk of packets. Thus, while the plastic intragranular fracture, which is characterized by very fine dimples, remains the main mechanism of fracture, the plasticity of steel is not reduced.

Figure 7 presents fractures of samples of 10Kh9V1M1FBR steel after impact tests. It can be seen that, in the temperature range of 20 to −20°C, completely plastic fracture is observed. The dimples are clearly visible at the surfaces of the fractures. Large dimples are formed at the grain-boundary $M_{23}C_6$ particles (≥100 nm) located at the boundaries of IAGs, martensite packets, and blocks. The sizes and shapes of the dimples are determined by the morphology and size of these particles. As a result, the sizes of the dimples vary in a wide range of 5–30 μm. The decrease in the test temperature increases the number of coarse dimples. At temperatures of −40°C, a transition from plastic to brittle transcrystalline fracture (the fraction of the plastic component is 60%) is observed and brittle fracture occurs according to the mechanism of quasi-cleavage [22]; the mixed-type fracture is also retained at −60°C. Regions of plastic dimpled fracture and brittle fracture are observed in the fractured surface; quasi-cleavage facets are connected by leaf-type tear ridges. Correspondingly, if the fracture is intragranular and regions of plastic fracture are observed, the impact toughness remains high (KCV_{-60} = 95 J/cm^2). A perceptible reduction in the impact toughness (30 J/cm^2) upon a decrease in the test temperature to −80°C is correlated with the disappearance of the plastic region in the fracture curve and a decrease in the fraction of the ductile component to 1%. The further drop in the impact toughness with decreasing temperature to −196°C is associated with the development of the intergranular fracture at the boundaries of IAGs and martensite packets. Thus, 10Kh9V1M1FBR steel retains impact toughness above the conditional level (20 J/cm^2), which characterizes the transition to fully brittle fracture [18] until it fails under impact loads due to transcrystalline quasi-cleavage. If, upon the propagation of the main crack, the plastic mechanism of fracture makes even a slight contribution to the overall fracture, the value of *KCV* will be sufficient to suppress the onset of fracture [18].

The FATT was determined based on the fraction of the plastic component and corresponds to −45°C. At this temperature, the fraction of the plastic component in the fracture is equal to 50%. It should be noted that the FATT coincides with the temperature of the BDT, at which the medium value between the values of the maximum and minimum impact toughnesses is observed (Fig. 8). Note that the minimum value of *KCV* = 40 J/cm^2, which should be at room temperature in order to ensure the reliable operation of both steam turbines and high-temperature circuits of boilers, as well as the main steam pipe, is observed at a temperature of about −70°C. Thus, 10Kh9V1M1FBR steel has a large reserve of fracture toughness.

DISCUSSION

An analysis of the above results shows that 10Kh9V1M1FBR steel demonstrates not only outstanding creep resistance [1], but also very good fracture toughness. Upon static loading, even small signs of brittle fracture according to the mechanism of pure cleavage, in which cracks propagate along {100} planes, has not been revealed down to the temperature of liquid nitrogen. This fracture mechanism leads to the formation of characteristic stair steps [22], which are often observed in pearlitic steels, even at room temperature [23]. Consequently, the investigated steel is not inclined to embrittlement upon static loading. The impact toughness of 10Kh9V1M1FBR steel upon dynamic loading is also high and even exceeds the same characteristic in a ferritic high-chromium steel at room temperature [24]. A clearly pronounced BDT is observed upon impact loading; however, this transition, which according to Eq. (1) should be observed at

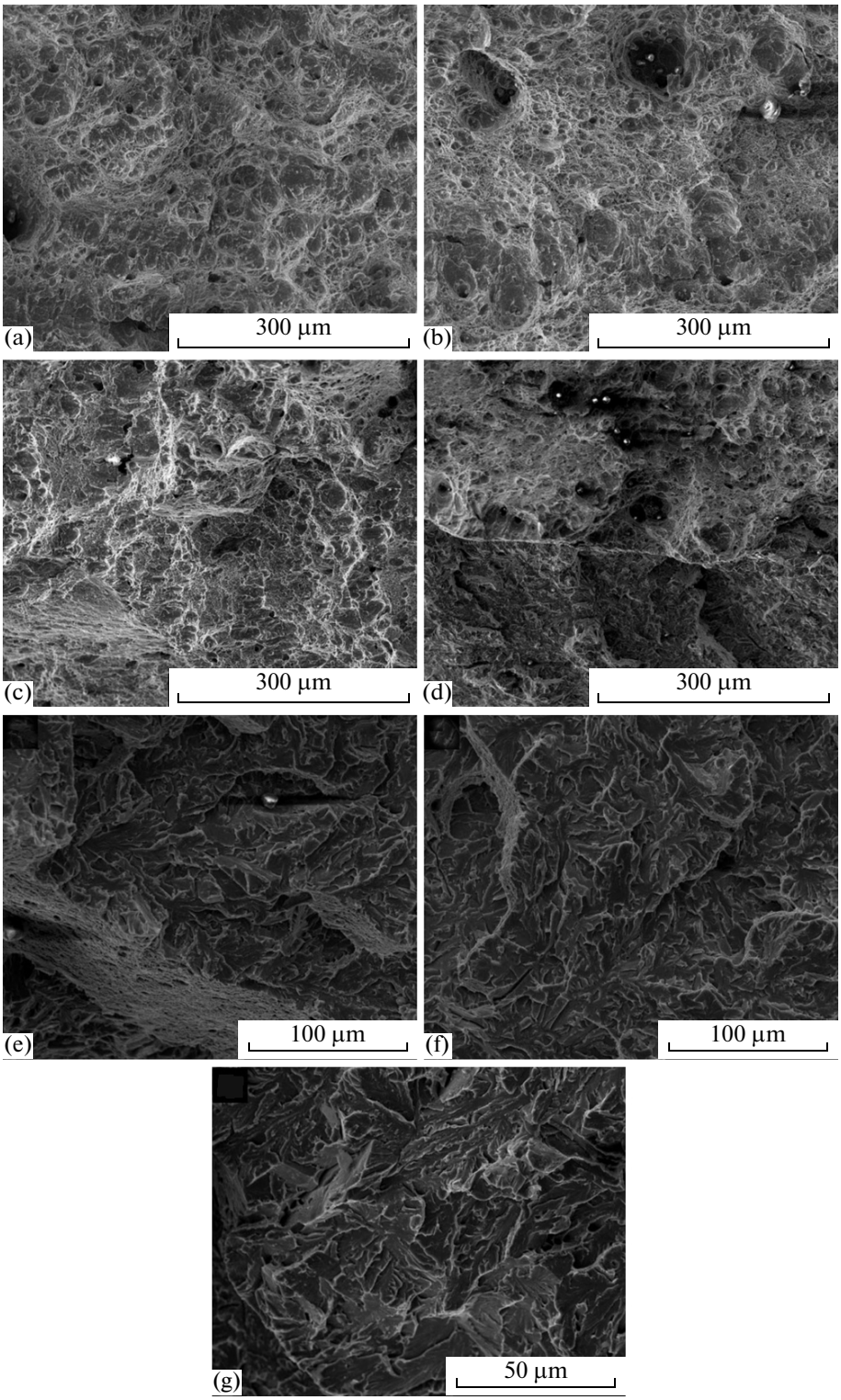

Fig. 7. Fractography of the fractures of 10Kh9V1M1FBR steel after impact tests at temperatures of (a) 20 (a), (b) 0, (c) −20, (d) −40, (e) −60, (f) −80, and (g) −196°C.

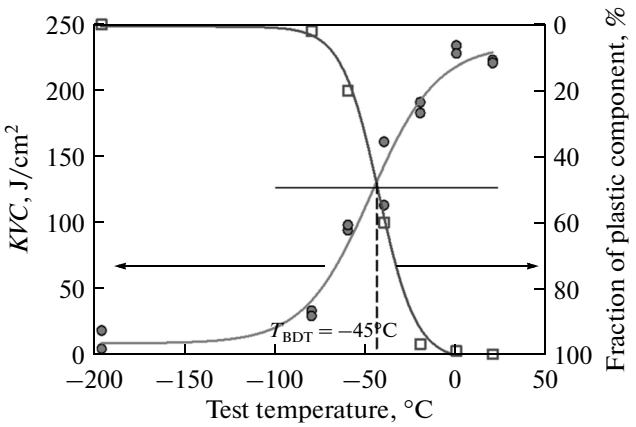

Fig. 8. Dependence of (●) impact toughness and (□) fraction of the plastic component on test temperature.

–90°C, is absent upon static loading. The lack of a correlation with the data obtained in tensile tests indicates that the brittle fracture of this material may only begin if a crack is present in a construction with a greater than critical size [18], and its loading has an impact character. Thus, BDT only takes place in 10Kh9V1M1FBR steel at the third stage of fracture, when the uncontrolled propagation of the main crack occurs [18]. At the first and second stages, when the formation of microcracks and their coalescence into a stable crack capable of growth occurs [18], the BDT is not observed down to –140°C.

Based on the data obtained, it is possible to give the following forecast for the embrittlement of steel during operation. At high temperature, the coarsening of grain-boundary $M_{23}C_6$ carbides occurs in 10Kh9V1M1FBR steel [25, 26]. Moreover, large Laves-phase particles (from 300 nm to 1 μm) precipitate at the boundaries of mainly IAGs and martensite packets [27] and facilitate the nucleation of microcracks at these boundaries. Upon static loading, this will not lead to embrittlement, since there are no processes that can lead to a transition from plastic to brittle fracture in the ferritic matrix [25–27]; i.e., only the fraction of intergranular fracture will increase, which, upon the predominance of intragranular fracture, does not significantly affect the fracture toughness [12].

In the case of the formation of continuous films at the boundaries of IAGs, with a drop in the *KCV* to 6 J/cm^2, a transition to brittle intergranular fracture is possible upon impact loading, even at room temperature [13]. However, in steels of this type, no continuous chains of $M_{23}C_6$ carbides and Fe_2W Laves phases are formed at the boundaries of IAGs upon creep [20, 25, 27]. Consequently, the plastic intragranular fracture will be observed [5] in any case that will provide a *KCV* value of 40 J/cm^2 and will allow one to use coal-fired power plants that use steel in their construction without any restrictions on life span. It is not possible to draw the same conclusion about the possibility of using 10Kh9V1M1FBR steel in reactor constructions. It is known that irradiation by neutrons leads to a strong embrittleness of the high-chromium steels [7–11], and there is no description in the open literature of the effects of irradiation on the fracture mechanism and BDT.

CONCLUSIONS

(1) The normalization and two-stage tempering of 10Kh9V1M1FBR steel lead to the formation of troostomartensite structure with grain-boundary $M_{23}C_6$ carbides and M(C,N) carbonitrides located in the ferrite matrix. The two-phase separation of the M(C,N) carbonitrides into V- and Nb-enriched carbonitrides takes place.

(2) The reduction in the temperature of static tensile test from 20 to –140°C leads to an increase in the yield stress by 33% and the ultimate tensile strength by 42%, while plasticity remains almost unchanged and is in the range of 20–25%. High uniform elongation is determined by the ratio of $\sigma_u/\sigma_{0.2} \sim 1.4$, which weakly depends on the temperature. At all test temperatures, plastic intragranular fracture is the main mechanism of fracture. The decrease in the temperature leads to an increase in the contribution of the intergranular mechanism of fracture related to the formation of microcracks at the grain-boundary $M_{23}C_6$ carbides. With decreasing temperature, the type of fracture changes from plastic to quasi-brittle.

(3) The clearly pronounced brittle–ductile transition, which is observed at the temperature of –45°C, is associated with the transition from plastic intragranular to quasi-brittle fracture. 10Kh9V1M1FBR steel shows a relatively high impact toughness down to a temperature of –60°C (95 J/cm^2). The impact toughness only drops to critical values (30 J/cm^2) as the temperature decreases to –80°C, which correlates with the decrease in the fraction of the plastic component on the fracture surface down to 1%. At a subsequent decrease in the temperature to –196°C, the impact toughness decreases by three times. This is connected with the transition from intragranular brittle fracture to intergranular fracture along the boundaries of initial austenite grains and martensite packets.

ACKNOWLEDGMENTS

This work was supported by the Russian Science Foundation (project no. 14-29-00173). We are grateful to the Center of Collaborative Access "Diagnostics of the Structure and Properties of Materials" of the Belgorod National Research University for supplying the equipment for structural studies and mechanical tests.

REFERENCES

1. F. Abe, T.-U. Kern, and R. Viswanathan, *Creep-Resistant Steels* (Woodhead, Boca Raton, FL, 2008).

2. R. O. Kaybyshev, V. N. Skorobogatykh, and I. A. Shchenkova, "New martensitic steels for fossil power plant: Creep resistance," Phys. Met. Metallogr. **109**, 186–200 (2010).
3. S. Sathyanarayanan, J. Basu, A. Moitra, G. Sasikala, and V. Singh, "Effect of thermal aging on ductile–brittle transition temperature of modified 9Cr–1Mo steel evaluated with reference temperature approach under dynamic loading condition," Metall. Mater. Trans. A **44**, 2141–2155 (2013).
4. X. Hu, L. Huang, W. Yan, W. Wang, W. Sha, Y. Shan, and K. Yang, "Evolution of microstructure and changes of mechanical properties of CLAM steel after long-term aging," Mater. Sci. Eng., A **586**, 253–258 (2013).
5. W. Zhong, W. Wang, X. Yang, W. Li, W. Yan, W. Sha, W. Wang, Y. Shan, and K. Yang, "Relationship between Laves phase and the impact brittleness of P92 steel reevaluated," Mater. Sci. Eng., A **639**, 252–258 (2015).
6. G. Sasikala and S. K. Ray, "Evaluation of quasistatic fracture toughness of a modified 9Cr–1Mo (P91) steel," Mater. Sci. Eng., A **479**, 105–111 (2008).
7. A.-A. F. Tavassoli, E. Diegele, R. Lindau, N. Luzginova, and H. Tanigawa, "Current status and recent research achievements in ferritic/martensitic steels," J. Nucl. Mater. **455**, 269–276 (2014).
8. P. Yvon and F. Carre, "Structural materials challenges for advanced reactor systems," J. Nucl. Mater. **385**, 217–222 (2009).
9. K. L. Murty and I. Charit, "Structural materials for Gen-IV nuclear reactors: Challenges and opportunities," J. Nucl. Mater. **383**, 189–195 (2008).
10. J. S. Cheon, C. B. Lee, B. O. Lee, J. P. Raison, T. Mizuno, F. Delage, and J. Carmack, "Sodium fast reactor evaluation: Core materials," J. Nucl. Mater. **392**, 324–330 (2009).
11. Th. S. Byun, J. H. Yoon, D. T. Hoelzer, Y. B. Lee, S. H. Kang, and S. A. Maloy, "Process development for 9Cr nanostructured ferritic alloy (NFA) with high fracture toughness," J. Nucl. Mater. **449**, 290–299 (2014).
12. A. Yu. Kipelova, A. N. Belyakov, V. N. Skorobogatykh, I. A. Shchenkova, and R. O. Kaibyshev, "Tempering-induced structural changes in steel 10Kh9K3V1M1FBR and their effect on mechanical properties," Met. Sci. Heat Treat. **52**, 100–110 (2010).
13. N. Dudova, R. Mishnev, and R. Kaibyshev, "Effect of tempering on microstructure and mechanical properties of boron containing 10% Cr steel," ISIJ Int. **51**, 1912–1918 (2011).
14. P. Yan, Zh. Liu, H. Bao, Y. Wenga, and W. Liu, "Effect of tempering temperature on the toughness of 9Cr–3W–3Co martensitic heat resistant steel," Mater. Des. **54**, 874–879 (2014).
15. L. Schafer, "Tensile and impact behavior of the reduced-activation steels OPTIFER and F82H Mod," J. Nucl. Mater. **283–287**, 707–710 (2000).
16. W. Yan, P. Hu, L. Deng, W. Wang, W. Sha, Y. Shan, and K. Yang, "Effect of carbon reduction on the toughness of 9CrWVTaN steels," Metall. Mater. Trans. A **43**, 1921–1933 (2012).
17. Th. S. Byun, J. H. Yoon, S. H. Wee, D. T. Hoelzer, and S. A. Maloy, "Fracture behavior of 9Cr nanostructured ferritic alloy with improved fracture toughness," J. Nucl. Mater. **449**, 39–48 (2014).
18. *ASM Handbook. Mechanical Testing and Evaluation* (ASM International, Materials Park, Ohio, 2000), vol. 8.
19. I. I. Gorbachev and V. V. Popov, "Thermodynamic simulation of the Fe–V–Nb–C–N system using the CALPHAD method," Phys. Met. Metallogr. **111**, 495–502 (2011).
20. V. Dudko, A. Belyakov, D. Molodov, and R. Kaibyshev, "Microstructure evolution and pinning of boundaries by precipitates in a 9 % Cr heat resistant steel during creep," Metall. Mater. Trans. A **44**, 162–172 (2013).
21. Y. Kimura, T. Inoue, F. Yin, and K. Tsuzaki, "Inverse temperature dependence of toughness in an ultrafine grain-structure steel," Science **320**, 1057–1058 (2008).
22. *ASM Handbook. Fractography* (ASM International, Materials Park, Ohio, 1987), vol. 12.
23. A. V. Makarov, R. A. Savrai, V. M. Schastlivtsev, T. I. Tabatchikova, and L. Yu. Egorova, "Mechanical properties and fracture upon static tension of the high-carbon steel with different types of pearlite structure," Phys. Met. Metallogr. **104**, 522–534 (2007).
24. I. L. Yakovleva, N. A. Tereshchenko, D. A. Mirzaev, A. V. Panov, and D. V. Shaburov, "Impact toughness and plastic properties of composite layered samples as compared to monolithic ones," Phys. Met. Metallogr. **104**, 203–211 (2007).
25. A. Kipelova, M. Odnobokova, A. Belyakov, and R. Kaibyshev, "Effect of Co on creep behavior of a P911 steel," Metall. Mater. Trans. A **44**, 577–583 (2013).
26. A. Kipelova, R. Kaibyshev, A. Belyakov, and D. Molodov, "Microstructure evolution in a 3% Co modified P911 heat resistant steel under tempering and creep conditions," Mater. Sci. Eng., A **528**, 1280–1286 (2011).
27. A. Kipelova, A. Belyakov, and R. Kaibyshev, "Laves phase evolution in a modified P911 heat resistant steel during creep at 923 K," Mater. Sci. Eng., A **532**, 71–77 (2012).

Translated by O. Golosova